Coupled structural-thermodynamic modelling of the molten salt system NaCl-UCl_3

van Oudenaren, G. I.L.; Ocadiz-Flores, J. A.; Smith, A. L.

DOI
10.1016/j.molliq.2021.117470

Publication date
2021

Document Version
Final published version

Published in
Journal of Molecular Liquids

Journal of Molecular Liquids 342 (2021) 117470

Contents lists available at ScienceDirect

Journal of Molecular Liquids

journal homepage: www.elsevier.com/locate/molliq

Coupled structural-thermodynamic modelling of the molten salt system NaCl-UCl_3

G.I.L. van Oudenaren, J.A. Ocadiz-Flores, A.L. Smith *

Delft University of Technology, Faculty of Applied Sciences, Radiation Science & Technology Department, Mekelweg 15, 2629 JB Delft, the Netherlands

ARTICLE INFO

Article history:
Received 14 May 2021
Revised 17 August 2021
Accepted 2 September 2021
Available online 13 September 2021

Keywords:
Molecular dynamics
Polarizable ion model
CALPHAD
Chloride salts
Molten salt reactors

ABSTRACT

Molten chloride salts are ionic liquids in which the anions and cations exhibit network formation. An attractive salt system for use in molten salt reactors is NaCl-UCl_3, an ionic liquid with complex non-ideal thermodynamic behaviour due to the formation of short-range order. The relationship between local structure and thermodynamic properties is investigated in this work, in which molecular dynamics simulations using the Polarizable Ion Model (PIM) and thermodynamic modelling by means of the CALPHAD method are combined. The system is simulated for a wide range of temperatures and compositions and various properties are derived derived from molecular dynamics data: density/molar volume, thermal expansion, heat capacity and excess properties including excess molar volume, mixing enthalpy and excess heat capacity. Generally, there is good agreement with previously published experimental data. An in depth analysis of the local structure of the liquid is performed for multiple temperatures. This analysis demonstrates the transition from a molecular liquid consisting of primarily Na^+, Cl^-, UCl_6^{3-}/UCl_7^{4-} at low UCl_3 content to a polymeric liquid at high UCl_3 content, manifesting itself in the formation of species like $U_2Cl_{12}^{6-}$, $U_3Cl_{17}^{8-}$, $U_4Cl_{22}^{10-}$ etc. Exceeding 40% UCl_3, the liquid consists of a three-dimensional network of corner or edge-sharing uranium polyhedra. The output of the MD simulations and experimental data are incorporated into a coupled structural-thermodynamic model for the NaCl-UCl_3 system based on the quasi-chemical formalism in the quadruplet approximation, that provides a physical description of the melt and reproduces (in addition to the thermodynamic data) the chemical speciation of uranium polymeric species predicted from the simulations.

1. Introduction

Chloride salts have attracted an increasing interest in recent years as fuel and coolant system for the next generation of nuclear fission Molten Salt Reactors (MSRs), in particular for designs with a fast spectrum. The NaCl-UCl_3 system is to this date a reference for a number of reactor concepts under development (e.g. Moltex Energy, Elysium Industries, TerraPower) [1–3]. UCl_3 serves as the primary fissile material, while NaCl is an attractive carrier salt due to its high solubility for actinides [4], availability and low cost. During irradiation, the chemical composition of the fuel continuously changes, however, as the fission process introduces new reactive dissolved, precipitated or gaseous species, depending on local thermodynamic equilibrium conditions. The MSR salt system is thus a complex multi-component system, that shows complex non-ideal thermodynamic behaviour at the high temperatures used in the reactor [4]. An exhaustive assessment through models and simulations codes of this dynamic and complex fuel physical chemistry (during normal operation and accidental conditions) is challenging, but also a stringent requirement for the safety analysis. As a first step, a thorough knowledge of the base salt NaCl-UCl_3 physico-chemical properties (i.e. heat capacity, melting temperature, density, viscosity, thermal conductivity etc.) is essential to accurately model the thermal behaviour.

Molecular dynamic studies of NaCl-UCl_3 have been performed using the Polarizable Ion Model (PIM) by Li et al. [5], in which the local structure, heat capacity, thermal conductivity and diffusivity were determined in the 5–55% UCl_3 composition range at 1100 K. A similar study was performed by Baty [6] for a small number of NaCl-UCl_3 compositions, pure NaCl and UCl_3 and some closely related compounds. This work expands both the composition and temperature range of the simulations previously done. In addition, the excess molar volume, thermal expansion, mixing enthalpy and excess heat capacity are determined for the first time, and are compared to experimental data where possible.

While the structures of liquid NaCl and UCl_3 have been studied in much detail [7,8], the relationship between the structural and

* Corresponding author.
E-mail address: a.l.smith@tudelft.nl (A.L. Smith).

https://doi.org/10.1016/j.molliq.2021.117470
0167-7322/

thermodynamic excess properties of the (Na,U)Cl_x salt system is relatively unexplored, despite the evident correlation. Molten chloride salts are ionic liquids in which the anions and cations exhibit network formation, depending on composition and temperature conditions. NaCl is a completely dissociated ionic melt, while UCl_3 can be qualified as a "polymeric" liquid, in which the coordination shells of uranium cations form corner, edge or face-sharing polyhedra by which the entire melt is interconnected. A mixture of the two end-members may go from a regime with molecular species to one where network formation is observed. In this work, the study of this network formation by means of molecular dynamics is coupled to the thermodynamics of the system using the CALPHAD method [9].

Two thermodynamic modelling assessments of the NaCl-UCl_3 system have been reported to this date: by Yin et al. using a substitutional solution model [10] and Beneš and Konings [11] using a quasi-chemical model in the quadruplet approximation. However, the aforementioned models do not account for the chemical speciation in the melt, as proposed herein, where the structural properties obtained from MD are subsequently used as input to develop a coupled structural-thermodynamic CALPHAD assessment of the NaCl-UCl_3 system, using a quasi-chemical type of formalism. The model proposed can describe simultaneously the phase equilibria, mixing enthalpy and speciation of the liquid, following the methodology recently applied to the LiF-BeF_2[12] and LiF-UF_4 systems [13].

2. Brief literature review

Phase diagram studies of the NaCl-UCl_3 system were performed as early as 1943 by Kraus [14] using differential thermal analysis (DTA), and more recently (2015) by Sooby et al. [15] using differential scanning calorimetry (DSC). Mixing enthalpy data were collected in 2002 by Matsuura et al. [16] at 1113 K using an argon filled calorimeter with the break-off ampoule technique. The aforementioned thermodynamic model of this system by Beneš and Konings [11] used the quasi-chemical formalism in the quadruplet approximation. This model did not account for the mixing enthalpy data of Matsuura et al. [16], however. The calculated mixing enthalpy shows a minimum around -4.5 kJ·mol^{-1} at x(UCl_3) ≈ 0.35, while the experimental data by Matsuura et al. [16] suggest this minimum to be located around -7.5 kJ·mol^{-1} at x(UCl_3) ≈ 0.50. The later model by Yin et al. [10] using the substitutional solution model accounted for the experimental mixing enthalpy data.

The structure of liquid NaCl was experimentally studied by Edwards et al. [7] at 1148 K using neutron diffraction from which the partial structure factors of Na-Na, Na-Cl and Cl-Cl were derived and used to calculate radial distribution functions. The structure of liquid UCl_3 was experimentally measured by Okamoto et al. [8] at 1200 K using X-ray diffraction by taking the Fourier transform of the reduced intensity function. The molecular dynamics simulations of Li et al. [5] (in 5–55% UCl_3 range at 1100 K using the polarizable ion model) revealed that the liquid mixture consists of mainly 6- and 7-fold coordinated uranium monomers at low UCl_3 fractions, after which network formation starts to take place and the liquid becomes entirely "polymerized" above 40% UCl_3.

Finally, the density of NaCl-UCl_3 mixtures was determined by Desyatnik et al. [17] using the maximum (argon) bubble pressure method, over the full composition range for temperatures between 900 and 1300 K. The same authors also determined the dynamic viscosity of NaCl-UCl_3 by investigating the dampening of oscillations in a salt-filled crucible under similar measurement conditions (composition, temperature range).

3. Methods

3.1. Molecular dynamics simulations: the polarizable ion model

The Polarizable Ion Model (PIM) used in this work has been very successful in simulating molten salts for a variety of systems (LiF-BeF_2, La/Tb/YCl_3, NaCl-UCl_3) [12,18,5]. The PIM potential is defined by four terms, namely a Coulombic charge-charge interaction V_{qq}, repulsive interaction V_{rep}, dispersive interaction V_{disp}, and a polarizable term V_{pol} which accounts for polarizability of the ions. The detail of each term is given in the Supplementary Information.

The PIM parameters used in this work (listed in the Supplementary Information) were determined by Madden et al. [19,20] and the U-Na dipole-dipole/quadrupole parameters were fine-tuned by Li et al. [5].

The assessed compositions and temperatures are listed in Table 1. The systems were equilibrated for 500 ps in the NpT ensemble at 10^{-8} a.u. pressure (2.94 bar), from which the equilibrium volumes were taken and molar enthalpies were determined. This was followed by 200 ps of equilibration in the NVT ensemble, and finally a 500 ps production run for each temperature and composition. All ensembles had a time step of 0.5 fs. The relaxation times of the Nosé-Hoover thermostat and barostat were set to 10 ps. Cut-offs for the real space part of the Ewald sum and short-range potential were both set to less than half the length of the cell, whereas the relaxation time for both the Nosé-Hoover thermostat and barostat (for the NpT run) was set to 10 ps.

3.2. Thermodynamic modelling

The thermodynamic modelling assessment of the NaCl-UCl_3 system was carried out using the CALPHAD (CALculation of Phase Diagram) method, based on the least-squares minimisation of the total Gibbs energy of the system [9] using the Factsage software (Version 7.0) [21]. Both the experimental phase diagram and mixing enthalpy data reported in the literature, and the output of the MD simulations were used to optimise the excess parameters of the Gibbs energy functions of the phases involved in this system.

3.2.1. Stoichiometric compounds

The Gibbs energy function of a pure condensed phase is defined as:

$$G(T) = \Delta_f H^o_m(298) - S^o_m(298K)T + \int_{298}^{T} C_{p,m}(T)dT - T\int_{298}^{T} \times \frac{C_{p,m}}{T}dT \quad (1)$$

where $\Delta_f H^o_m(298)$ is the standard enthalpy of formation, $S^o_m(298K)$ is the standard absolute entropy, both evaluated at a standard temperature of 298.15 K (noted 298 K throughout this work for simplicity), and $C_{p,m}$ is the isobaric heat capacity, expressed with a polynomial function:

$$C_{p,m}(T) = a + bT + cT^2 + dT^{-2} \quad (2)$$

The NaCl-UCl_3 is a simple eutectic system. The thermodynamic properties of the end-members, listed in Table 2 were taken from the IVTAN tables for NaCl(cr,l) [22], and the recent review of Capelli and Konings for UCl_3(cr,l) [23]. The heat capacity of UCl_3(l) is reported equal to 129.7 J·K^{-1}·mol^{-1} in the latter review. In this work, we have taken the heat capacity value obtained from the MD simulations, i.e. 151.1 J·K^{-1}·mol^{-1}, in better agreement with the evolution observed for the (Na,U)Cl_x liquid solution (see Section 4.1.4). The choice of the heat capacity data for NaCl(l) requires a bit more discussion. The data selected in the IVTAN tables by Glushko et al. [22], i.e. (67.9 ± 1.0) kJ·mol^{-1} is the average

Table 1
Simulated ensembles in MD simulations of the NaCl-UCl_3 system. $x(UCl_3)$ is the molar fraction of UCl_3.

$x(UCl_3)$	N_{Cl^-}	$N_{U^{3+}}$	N_{Na^+}	N_{total}	T/K
0	320	0	320	640	1100/1200/1300/1400
0.049	334	15	289	638	1100/1200/1400
0.10	348	29	261	638	1100/1200/1400
0.148	360	41	237	638	1100/1200/1400
0.199	372	53	213	638	1100/1200/1400
0.251	383	64	191	638	1100/1200/1400
0.302	393	74	171	638	1100/1200/1400
0.352	402	83	153	638	1100/1200/1400
0.399	410	91	137	638	1100/1200/1400
0.45	418	99	121	638	1100/1200/1400
0.498	425	106	107	638	1100/1200/1300/1400
0.595	438	119	81	638	1100/1200/1300/1400
0.697	450	131	57	638	1100/1200/1300/1400
0.802	461	142	35	638	1100/1200/1300/1400
0.899	470	151	17	638	1100/1200/1300/1400
1	480	160	0	640	1100/1200/1300/1400

Table 2
Thermodynamic data for end-members used in this work for the thermodynamic assessment: $\Delta_f H^o_m(298\ K)/(kJ \cdot mol^{-1})$, $S^o_m(298\ K)/(J{\cdot}K^{-1}{\cdot}mol^{-1})$, and heat capacity coefficients $C_{p,m}(T/K)/(J{\cdot}K^{-1}{\cdot}mol^{-1})$, where $C_{p,m}(T/K) = a + b{\cdot}T + c{\cdot}T^2 + d{\cdot}T^{-2}$. Optimized data are shown in **bold**.

Compound	$\Delta_f H^o_m(298\ K)/$	$S^o_m(298\ K)/$	$C_{p,m}(T/K)/(J{\cdot}K^{-1}{\cdot}mol^{-1}) = a + b{\cdot}T + c{\cdot}T^2 + d{\cdot}T^{-2}$				T/K	Reference
	$(kJ{\cdot}mol^{-1})$	$(J{\cdot}K^{-1}{\cdot}mol^{-1})$	a	b	c	d		
NaCl(cr)	−411.260	72.15	47.72158	0.0057	$1.21466{\cdot}\ 10^{-5}$	−882.996	298.15–1074	[22]
NaCl(l)	−383.060	98.407	47.72158	0.0057	$1.21466{\cdot}\ 10^{-5}$	−882.996	298.15–1074	[22]
			68				1074–2500	This work
UCl_3(cr)	−863.700	163.9	106.967	−0.02086	$3.639{\cdot}\ 10^{-5}$	−129900	298.15–1115	[23]
UCl_3(l)[a]	−846.616	152.919	**151.1**				298.15–2500	[23], This work
U_2Cl_6(l)[a]	−1693.232	305.838	**302.2**				298.15–2500	This work

[a] Liquid uranium chloride is modelled as a $\{U_2Cl_6(l)\text{-}U^{VI}Cl_2(l)\text{-}U^{VII}Cl_2(l)\}$ mixture with $g^o_{U_{VI}Cl_2(l)} = 1/2\ g^o_{U_2Cl_6(l)} + 150000$ and $g^o_{U_2Cl_6(l)} = 1/2\ g^o_{U_2Cl_6(l)} + 150000$ (see Supplementary Information).

value from three studies reported in 1935 (68.1 $kJ{\cdot}mol^{-1}$, 1123–1268 K) [24], 1906 (66.6 $kJ{\cdot}mol^{-1}$, 1112–1205 K) [25], and 1977 (69 $kJ{\cdot}mol^{-1}$) [26]. Glushko et al. rejected, however, the data of Dawson et al. [27] collected in 1963, that are the data retained in the JANAF review [28]. Glushko et al. argue that the data measured between 1078 and 1279 K yield a heat capacity value between 73 and 87 $kJ{\cdot}mol^{-1}$. We have re-analysed the data of Dawson et al. [27] in this work, and have obtained 68.4 $kJ{\cdot}mol^{-1}$. It is thus not clear where the discrepancy pointed out in the analysis of Glushko et al. comes from. For the present thermodynamic model, we recommend to select the average value from the four studies, including that of Dawson et al., which yields (68.0 ± 1.0) $kJ{\cdot}mol^{-1}$. NaCl (cr) melts at (1074 ± 1) K with an enthalpy of fusion equal to (28.2 ± 0.2) $kJ{\cdot}mol^{-1}$ [22], while UCl_3(cr) melts at (1115 ± 2) K with an associated enthalpy of fusion equal to (49.0 ± 2.0) $kJ{\cdot}mol^{-1}$ [23].

3.2.2. Liquid solution

The excess Gibbs energy terms of the liquid solution are modelled in this work using the modified quasi-chemical model proposed by Pelton et al. [29] in the quadruplet approximation. Moreover, a coupled structural-thermodynamic description of the melt is made following the principles described by Smith et al. [12] to reflect the fact that mixtures rich in UCl_3 (>40% UCl_3 fraction) are found to be "polymeric", meaning that the melt entirely consists of species with a nucleation of more than 4. A detailed description of the quasi-chemical formalism and the implementation of the structural-thermodynamic model is described in the Supplementary Information.

In this work, the liquid solution is modelled to consist of chlorine anions Cl^-, sodium cations Na^+, and U^{3+}_{VI}, U^{3+}_{VII} and U^{6+}_2 cations, which are uranium monomers with coordinations [VI] and [VII] (i.e. UCl_6^{3-} and UCl_7^{4-}), respectively, and a dimer species with coordination [XII]. The U^{6+}_2 cations thus correspond to the $U_2Cl_{12}^{6-}$ species. The choice of these species is based on the wish to use a physical representation of the melt, while keeping a reasonable number of excess Gibbs energy parameters to be optimised. The $U_2Cl_{12}^{6-}$ species is assumed to represent the largest polymeric unit in the thermodynamic model. This means that UCl_3 is modelled as a connected network made entirely of dimers.

The optimised Gibbs energies values, also listed in the Supplementary Information, were obtained by fitting simultaneously the parameters of the thermodynamic model to the MD speciation data, experimental mixing enthalpy data [16] and experimental phase diagram data [15,14].

4. Results and discussion

4.1. Structural, thermophysical and thermochemical properties from MD simulations

4.1.1. Density and molar volume

The density and the molar volume of binary mixtures of NaCl-UCl_3 were calculated based on the average dimensions of the NpT ensemble simulation cells (500 ps equilibration time, 0 GPa pressure). The results are shown in Fig. 1a, in which they are compared to the reported equation by Li et al. [5] at identical conditions, and to the reported experimental density results by Desyatnik et al. [17] (Note: the data by Desyatnik et al. at the UCl_3 composition were extrapolated beyond the prescribed temperature range). The agreement is very good near the end-members, but there is a slight discrepancy near $x(UCl_3) = 0.5$ molar fraction. However, the difference does not exceed 6% which is acceptable and comparable to other MD studies [5,12,30,31]. The density results of Desyatnik et al. [17] and van Artsdalen and Yaffe

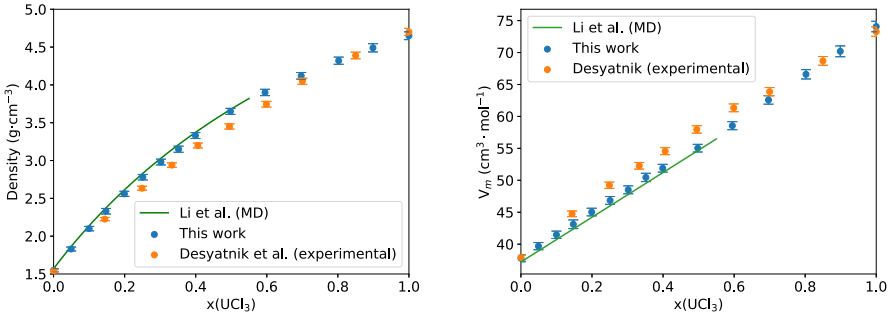

Fig. 1. Evolution of the (a) density and (b) molar volume of the (Na,U)Cl_x melt at T = 1100 K as function of molar fraction of UCl_3. The molecular dynamics results of this work are compared to experimental data by Desyatnik et al. [17] and simulations by Li et al. [5]. Errors on the data from this work are standard deviations of the calculated MD values; the error on the data of Desyatnik is 1% as taken from the corresponding paper [17].

for pure NaCl [32] over the full range of reported temperatures are compared to the results of this work in Fig. 2. Overall, the agreement is similar to the one just described at T = 1100 K. The temperature dependencies of the calculated density data at various compositions are comparable (i.e. similar slopes on the linear equations).

The evolution of the molar volume over all simulated compositions and temperatures is shown in Fig. A.1 in the Appendix. Linear equations fitted to the data points are listed in Table 3.

The excess molar volume calculated at 1100 K is shown in Fig. 3, where it is compared to the data obtained with the experimental results of Desyatnik et al. [17]. The behaviour observed from the experimental data, i.e. positive deviation in an almost parabolic fashion, is not reproduced in the MD simulations. Instead, the molar volume shows a subtle S-shape, with a nearly ideal behaviour up to $x(UCl_3)$ = 0.25 molar fraction, and a negative deviation above the latter composition. This behaviour coincides with the network formation of the liquid, which is described in Section 4.1.3, and causes the liquid to "contract". A negative deviation in the excess molar volume was also observed for the LiF-BeF_2 system [12], where extensive polymerization occurs.

4.1.2. Thermal expansion

Based on the calculated molar volumes, the thermal expansion of the liquid was also derived from the relation:

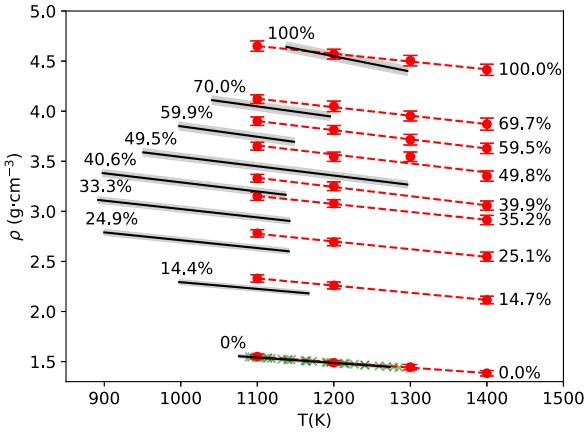

Fig. 2. Density of (Na,U)Cl_x melt as function of temperature at various molar fractions in UCl_3. Molecular dynamics results of this work (red) compared to the experimental data by Desyatnik et al. [17] (black; the grey regions around the black lines indicate the reported 1% experimental uncertainty) and van Artsdalen and Yaffe [32] (green). Errors on the data from this work are standard deviations of the calculated MD values; the error on the data of Desyatnik is 1% as taken from the corresponding paper [17].

Table 3
Molar volume of (Na,U)Cl_x melt as function of fraction UCl_3 for different temperatures.

T(K)	V_m [$cm^3 \cdot mol^{-1}$]
1100	37.743 + 0.359 $x(UCl_3)$
1200	39.166 + 0.356 $x(UCl_3)$
1300	40.261 + 0.361 $x(UCl_3)$
1400	42.201 + 0.355 $x(UCl_3)$

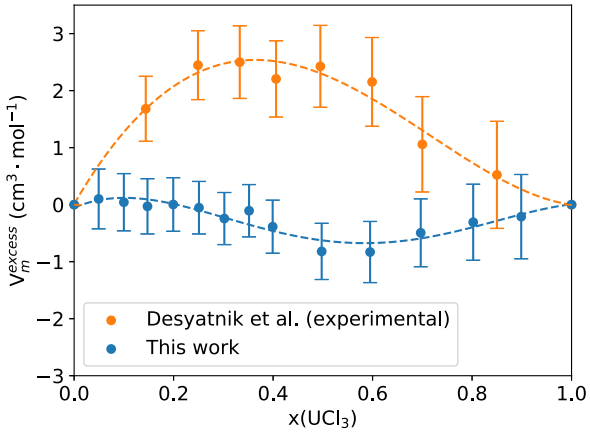

Fig. 3. Excess molar volume of the (Na,U)Cl_x melt at T = 1100 K as function of molar fraction UCl_3, compared to the values calculated from the experimental density data by Desyatnik et al. [17]. Errors on the data from this work are standard deviations of the calculated MD values; the error on the data of Desyatnik is 1% as taken from the corresponding paper [17].

$$\beta = \frac{1}{V_m}\left(\frac{\partial V_m}{\partial T}\right)_p \tag{3}$$

The results are shown in Fig. 4. The evolution is quasi-linear and the fitting equations are listed in Table 4. The thermal expansion shows a positive temperature dependence as expected, and decreases with increasing UCl_3 content: the stronger U-Cl bonds and increasing chloride bridging at high UCl_3 concentrations result in a decreased expansion compared to NaCl-rich salts.

4.1.3. Local structure

The calculated radial distribution functions (RDFs) of NaCl are compared to those derived from experimental neutron diffraction measurements by Edwards et al. [7] in Fig. 5a. The agreement on the intensity and radial distances is generally very good, although

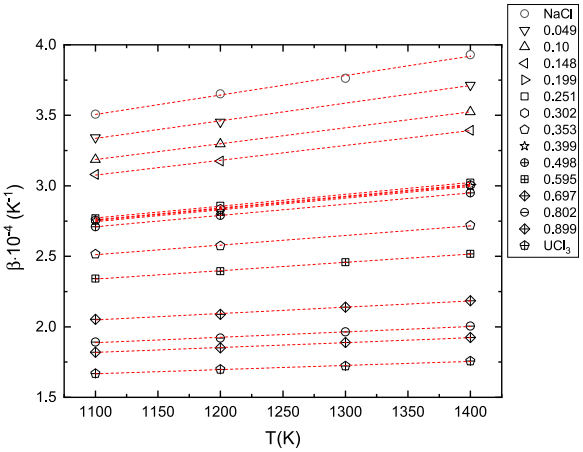

Fig. 4. Thermal expansion of the $(Na,U)Cl_x$ melt at various temperatures and compositions as derived from the MD simulations.

Table 4
Thermal expansion of the $(Na,U)Cl_x$ melt as function of temperature for different fractions in UCl_3.

x(UCl_3)	β (K^{-1})
0	$1.378 \cdot 10^{-7}T + 1.991 \cdot 10^{-4}$
0.049	$1.247 \cdot 10^{-7}T + 1.965 \cdot 10^{-4}$
0.10	$1.129 \cdot 10^{-7}T + 1.944 \cdot 10^{-4}$
0.148	$1.050 \cdot 10^{-7}T + 1.921 \cdot 10^{-4}$
0.199	$8.342 \cdot 10^{-8}T + 1.842 \cdot 10^{-4}$
0.251	$8.408 \cdot 10^{-8}T + 1.846 \cdot 10^{-4}$
0.302	$8.318 \cdot 10^{-8}T + 1.840 \cdot 10^{-4}$
0.352	$6.863 \cdot 10^{-8}T + 1.756 \cdot 10^{-4}$
0.399	$8.287 \cdot 10^{-8}T + 1.835 \cdot 10^{-4}$
0.498	$8.027 \cdot 10^{-8}T + 1.827 \cdot 10^{-4}$
0.595	$5.894 \cdot 10^{-8}T + 1.691 \cdot 10^{-4}$
0.697	$4.483 \cdot 10^{-8}T + 1.556 \cdot 10^{-4}$
0.802	$3.838 \cdot 10^{-8}T + 1.465 \cdot 10^{-4}$
0.899	$3.500 \cdot 10^{-8}T + 1.433 \cdot 10^{-4}$
1	$2.931 \cdot 10^{-8}T + 1.345 \cdot 10^{-4}$

the MD data seem to miss some of the features of the experimental curves.

The RDFs of UCl_3 are compared to those derived from experimental measurements by Okamoto et al. [8] in Fig. 5b. There is a near perfect overlap between the MD curve and the experimental one. The only difference is a slight shift of the radial distances of the maxima of the U-U and U-Cl curves, meaning that the location of the first coordination shell is slightly overestimated in the simulations. The evolution of the RDFs as a function of composition in NaCl-UCl_3 mixtures is shown in Fig. 6. The shape of the distributions changes significantly with UCl_3 fraction. Firstly in the U-Cl RDF, the intensity of the first coordination shell decreases, while the second coordination shell moves to lower radial distances. The reason for this behaviour is the formation of molecular species responsible for the shortening of the mean U-Cl distance. In the U-U RDF, the largest peak is initially located around 8.1 Å for low UCl_3 contents, corresponding to a melt consisting primarily of monomers. As the UCl_3 fraction increases, the intensity of the second coordination shell decreases, while the first coordination shell simultaneously becomes sharper. This is again the result of the network formation in the liquid. A more in depth analysis of the effects on coordination and chemical speciation is discussed next.

The chemical speciation of the liquid is determined from the calculated radial distribution functions. The first local minimum of the U-Cl RDFs is taken to be a bond cut-off distance. The chlorine anions that are located at a shorter distance than this bond cut-off distance are considered to be part of the first coordination shell of uranium. Moreover, if a chlorine anion is simultaneously part of the coordination shell of two uranium cations, and the corresponding U-U distance is less than two U-Cl distances, a U-Cl-U linkage is identified. The results of this analysis, i.e. the coordination environment and chemical speciation of $(Na,U)Cl_x$ melts as function of composition at T = 1100 and 1400 K are shown in Figs. 7 and 8, respectively.

At low UCl_3 content (below 10% UCl_3), the melt is largely dissociated. However, a significant fraction of uranium cations also forms dimers, reaching a fraction around 25% at a UCl_3 concentration of 10%. Above 10% UCl_3, rapid network formation (polymerisation) sets in, and at 40% UCl_3 concentration the melt is fully "polymerised". The coordination of the monomers starts out almost evenly distributed between 6- and 7-fold coordination at low UCl_3 content, with a small portion of 8-fold coordinated uranium ions. The results at 1100 K are in good agreement with those by Li et al. [5], while the results at T = 1400 K are reported for the first time. It is worth noting that the formation of UCl_5^{2-} complexes, as suggested by Desyatnik et al. [17] in relation with the positive deviation from ideal behaviour of the molar volumes and the obtained viscosity data, is not corroborated by the present results. The concentration of UCl_5^{2-} species is found to be marginal instead. With increasing temperature, the 6-fold coordination becomes (even) more prevalent than 7-fold and 8-fold coordinations as shown in Fig. 7. The temperature seems to have a limited effect

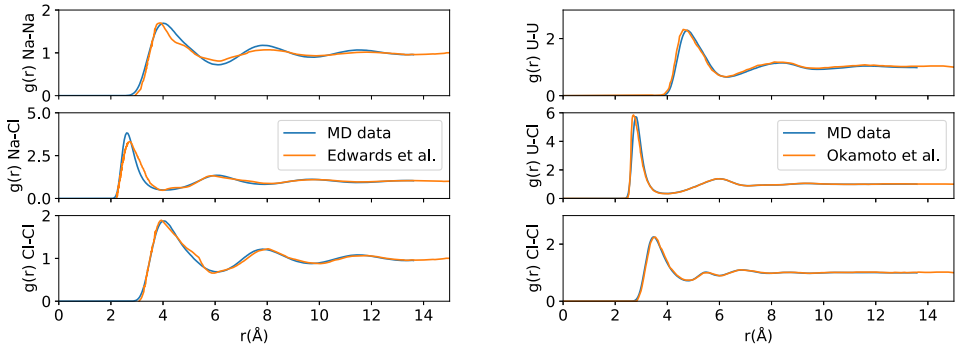

(a) NaCl (b) UCl_3

Fig. 5. (a) Radial distribution functions of NaCl: molecular dynamics simulation results at T = 1100 K compared to experimentally derived values (1148 K) by Edwards et al. [7]. (b) Radial distribution functions of UCl_3: molecular dynamics simulation results at T = 1200 K compared to experimentally derived values (1200 K) by Okamoto et al. [8].

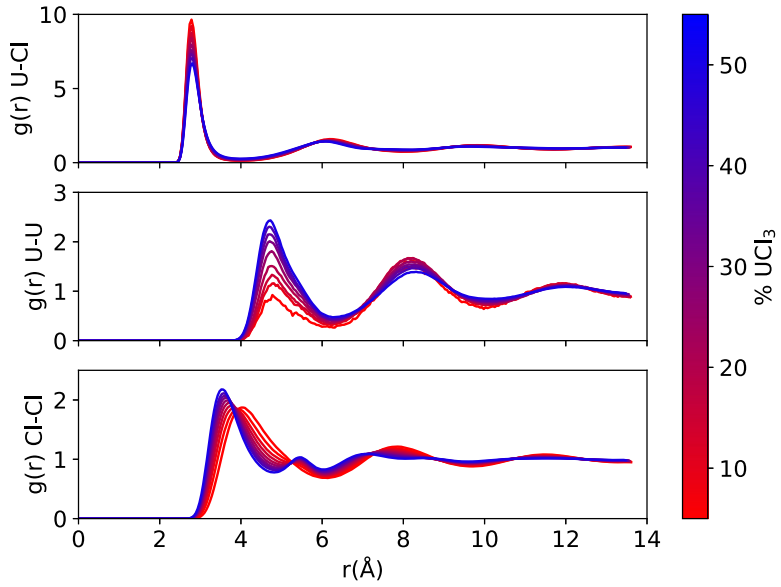

Fig. 6. Evolution of the U-Cl, U-U and Cl-Cl radial distribution functions in $(Na,U)Cl_x$ melts as function of composition at T = 1100 K.

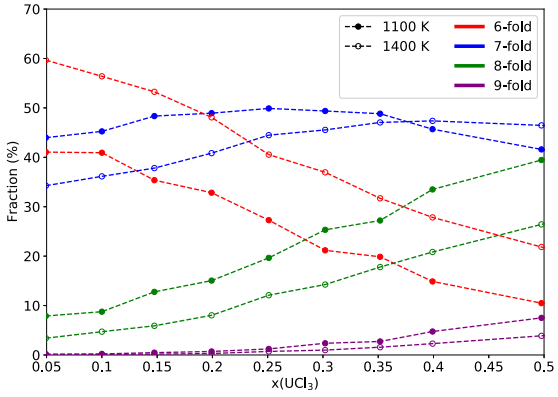

Fig. 7. Evolution of the fraction of UCl_6^{3-}, UCl_7^{4-}, UCl_8^{5-}, UCl_9^{6-} species as function of composition at T = 1100 and 1400 K.

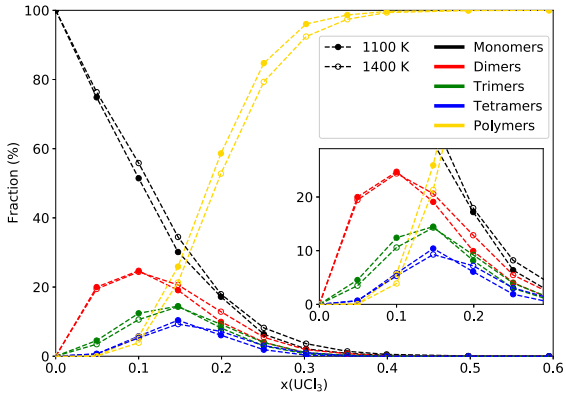

Fig. 8. Fraction of U atoms involved in monomers, dimers, trimers, tetramers and "polymers" as function of composition at T = 1100 and 1400 K; the designation "polymer" corresponds to a cluster with U nuclearity greater than 4.

on the mechanisms of network formation, however, as seen in Fig. 8. The network formation sets in only at a slightly lower rate with increasing temperature. This behaviour is nevertheless to be expected, since by increasing the temperature the density of the liquid decreases, which increases the distance between uranium ions. The U-U, U-Cl and Cl-Cl RDFs calculated at 15% UCl_3 concentration, shown in the Appendix (Fig. B.1), reflect this: increasing temperature decreases the height of the U-U coordination shells and increases their radial distance.

4.1.4. Thermodynamic properties

Heat capacity and mixing enthalpy of the $(Na,U)Cl_x$ melt were derived from the MD simulations, based on the calculated enthalpies, i.e. from the (average) potential energy of the production runs in the NpT ensemble.

The heat capacity was determined by fitting a linear equation to the enthalpy data obtained over the four different temperatures simulated (1100, 1200, 1300, 1400 K) using weighted linear regression analysis which accounted for the uncertainty in the determined enthalpy values.

$$C_{p,m} = \left(\frac{\partial H_m}{\partial T}\right)_p \tag{4}$$

The result is shown in Fig. 9a and is compared to other MD studies by Baty [6] and Li et al. [5], experimental data selected by Chase et al. (JANAF) [28], and an estimation by Beneš and Konings [11] for pure UCl_3. There is good agreement with both the MD data fit proposed by Li et al. [5] and the UCl_3 estimation by Beneš and Konings [11]. A rather large difference is observed between the UCl_3 data point obtained in this work and that of Baty [6], but since Baty did not report the associated uncertainty it is difficult to assess this discrepancy. The excess heat capacity is shown in Fig. 9b. It is slightly negative up to 60% UCl_3, after which a large negative deviation occurs, with a maximum deviation of about 7 $J{\cdot}K^{-1}{\cdot}mol^{-1}$ slightly above $x(UCl_3)$ = 0.8. This behaviour is also observed in other molten salt systems, notably the NaF-ThF_4 system, albeit at different component ratios [33]. This phenomena was explained by the disruption of the highly connected network of the pure ThF_4 end-member upon addition of Na^+ cations, resulting in a reduced heat capacity. The negative excess heat capacity was moreover related to the calculated negative excess thermal expansion, as both properties are linked to the vibrational contribution to the free energy, which is in this case lower than for an ideal mixture. A similar interpretation also stands for the NaCl-UCl_3 system.

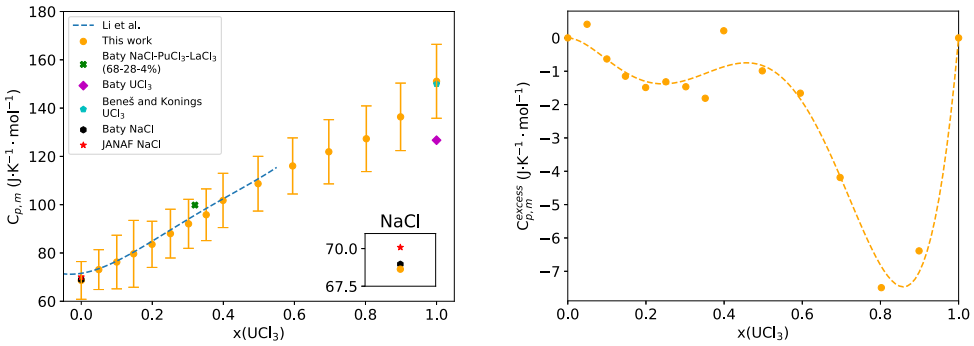

(a) $C_{p,m}$ (b) $C_{p,m}^{excess}$

Fig. 9. (a) Calculated heat capacity of $(Na,U)Cl_x$ melt as function of UCl_3 fraction. Other values reported in the literature are added for comparison [5,6,11,28]. (b) Excess heat capacity of $(Na,U)Cl_x$ melt as function of UCl_3 fraction with a polynomial fitted through the data points. Errors on this work (and the values themselves) were calculated using weighted linear regression on the mean and standard deviation of the (molar) enthalpy MD data.

The calculated mixing enthalpy (Eq. 5) at T = 1100 K is shown in Fig. 10, and compared to the experimental data by Matsuura et al. [16]. The calculated mixing enthalpy at other temperatures are shown in the Appendix (Fig. C.1).

$$\Delta_{mix}H_m^o(T) = H_m^o(T) - x(UCl_3)H_m^o(UCl_3,T) - (1 - x(UCl_3))H_m^o(NaCl,T) \quad (5)$$

A significant discrepancy is observed between the simulated and experimental results. The shape of the mixing enthalpy curve is identical, but the magnitude is around twice as large in the simulations. This might be an indication that the potential parameters (U-Cl, U-U, U-Na) could be further fine-tuned to better represent the thermodynamics of the liquid. (Absolute) overestimation of the mixing enthalpy in molecular dynamics data has been observed in similar molten salt systems, e.g. LiF-BeF_2 [12], LiF-UF_4 [13] and NaF-ThF_4 [33].

4.2. Coupled structural-thermodynamic model

The molecular dynamics speciation data are finally combined with the experimental phase equilibria [14,15] and mixing enthalpy [16] data for the development of a coupled structural-thermodynamic model using the methodology described in Section 3.2.2 and in the Supplementary Information. The calculated phase diagram is in good agreement with the phase diagram equilibrium data by Kraus et al. [14] and Sooby et al. [15] (see Fig. 11).

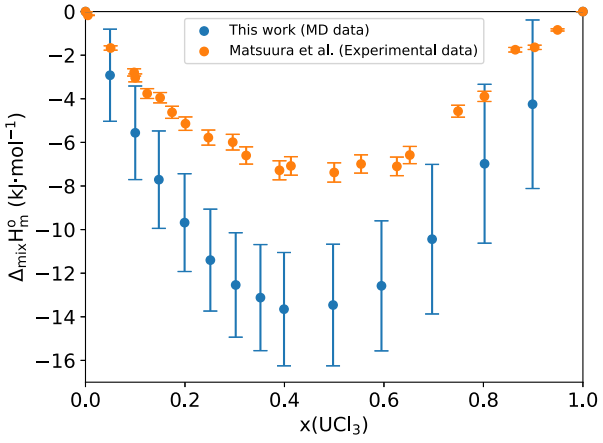

Fig. 10. Enthalpies of mixing calculated at T = 1100 K, and comparison to the experimental data by Matsuura et al. [16]. The uncertainty on the mixing enthalpy was calculated using the law of propagation of uncertainty. The uncertainty on the experimental data by Matsuura et al. was reported to be 6%.

The eutectic equilibrum is calculated to be at a composition of $x(UCl_3)$ = 0.349 and T = 792 K, which is in good agreement with Kraus who reports an eutectic composition around $x(UCl_3)$ = 0.33 and T = (793 ± 5) K, and with Sooby et al. [15] who reports $x(UCl_3)$ = (0.34 ± 0.02) and T = (796 K ± 2) K.

The mixing enthalpies calculated from the model are compared to the experimental data by Matsuura et al. [16] in Fig. 12. There is good agreement in both the shape and magnitude of the data.

The distribution of the uranium species $[U_{VI}\ Cl_6]^{3-}$, $[U_{VII}\ Cl_7]^{4-}$ and $[U_2Cl_{12}]^{6-}$ are finally calculated at T = 1100 and 1400 K based on the molar fractions of the quadruplets according to the following relations:

$$[U_{VI}Cl_6]^{3-} = \frac{X_{NaU_{VI}} + X_{U_{VI}U_{VI}} + X_{U_{VI}U_{VII}}/2 + X_{U_{VI}U_2}/2}{\sum_k \sum_{l>k} X_{kl/Cl_2} - X_{NaNa}} \quad (6)$$

$$[U_{VII}Cl_7]^{4-} = \frac{X_{NaU_{VII}} + X_{U_{VII}U_{VII}} + X_{U_{VI}U_{VII}}/2 + X_{U_{VII}U_2}/2}{\sum_k \sum_{l>k} X_{kl/Cl_2} - X_{NaNa}} \quad (7)$$

$$[U_2Cl_{12}]^{6-} = \frac{X_{NaU_2} + X_{U_2U_2} + X_{U_{VI}U_2}/2 + X_{U_{VII}U_2}/2}{\sum_k \sum_{l>k} X_{kl/Cl_2} - X_{NaNa}} \quad (8)$$

in which k and l are elements of the cation set $\{Na^+, U_{VI}^{3+}, U_{VII}^{3+}, U_2^{6+}\}$, and X_{kl} represents the mole fraction of the (k-Cl-l) quadruplet (see Supplementary Information for more detail on the quasi-chemical formalism).

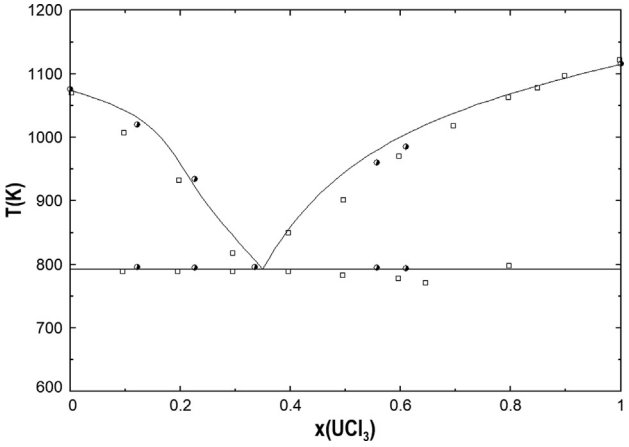

Fig. 11. Calculated phase diagram of the NaCl-UCl_3 system and comparison with the experimental data by Sooby et al. [15] (•) and Kraus [14] (□).

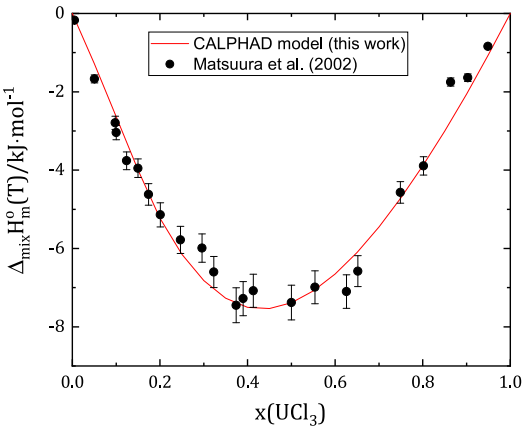

Fig. 12. Calculated enthalpy of mixing for the (Na,U)Cl_x melt at T = 1113 K, and comparison with the experimental data by Matsuura et al. [16].

As discussed in Section 3.2.2, the MD speciation is simplified by assuming the dimer species ($U_2Cl_{12}^{6-}$) includes all polymeric species with a nuclearity higher than 2 so as to keep the number of fitting parameters from growing too large. The results at T = 1100 K and 1400 K are shown in Figs. 13a and b, and compared to the results from MD simulations, with good agreement. The model captures the increasing contribution of 6-fold coordinated monomers with increasing temperature, which is the result of the decreasing density.

5. Conclusions

Using molecular dynamics simulations with the polarizable ion model, several thermo-physical properties of the NaCl-UCl_3 salt system have been determined, namely density/molar volume, thermal expansion, heat capacity, and excess properties including excess molar volume, mixing enthalpy and excess heat capacity. The information on the thermal expansion, heat capacity, and mixing enthalpy has been determined over the full compositional range for the first time. While there is good agreement with the available experimental data in most cases, some notable differences are observed in the excess properties. In particular, the calculated mixing enthalpy shows a similar shape but has a magnitude twice as large as the experimental data. These deviations might indicate that fine-tuning of the PIM parameters are necessary in order to produce more accurate results. Nevertheless the PIM does give useful insights into the structure of the liquid which has successfully been determined over a large temperature range for the first time. Moreover, a coupled structural-thermodynamic model has been developed with potential applicability to calculations related to MSR chemistry and pyroprocessing schemes, that reproduces the distribution of UCl_6^{3-}, UCl_7^{4-} and $U_2Cl_{12}^{6-}$ species in the melt in addition to the phase equilibrium and mixing enthalpy data.

CRediT authorship contribution statement

G.I.L. van Oudenaren: Conceptualization, Methodology, Investigation, Formal analysis, Validation, Data Curation, Visualisation, Writing – original draft. **J.A. Ocadiz-Flores:** Conceptualization, Methodology, Investigation, Validation, Data Curation, Supervision, Writing – review & editing. **A.L. Smith:** Conceptualization, Methodology, Investigation, Validation, Data Curation, Visualisation, Supervision, Funding acquisition, Resources, Project Administration, Writing – review & editing.

Declaration of Competing Interest

The authors declare that they have no known competing financial interests or personal relationships that could have appeared to influence the work reported in this paper.

Appendix A. Molar volumes

A.1

Appendix B. Radial distribution functions

B.1

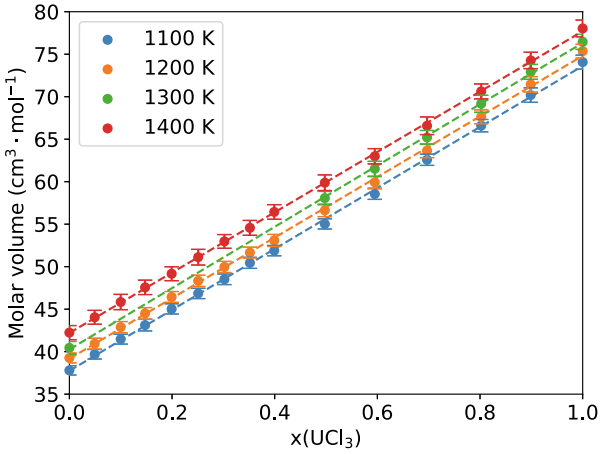

Fig. A.1. Molar volume of (Na,U)Cl_x melt at T = 1100, 1200, 1300, 1400 K as function of molar fraction UCl_3. The dotted lines are a linear fit of the data points.

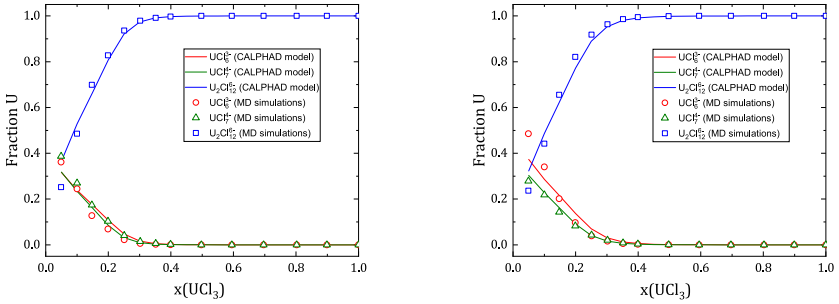

Fig. 13. Distribution of UCl_6^{3-}, UCl_7^{4-} and $U_2Cl_{12}^{6-}$ species calculated at (a) T = 1100 K and (b) T = 1400 K using the thermodynamic model compared to the results from MD simulations.

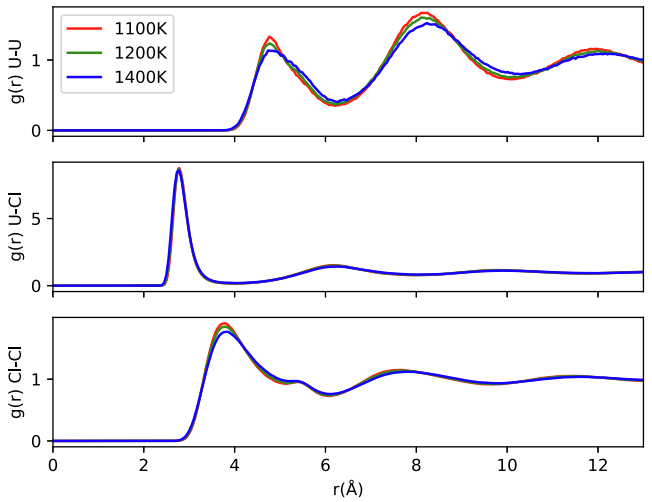

Fig. B.1. Evolution of the U-U, U-Cl and Cl-Cl radial distribution functions at 15% UCl_3 content as a function of temperature.

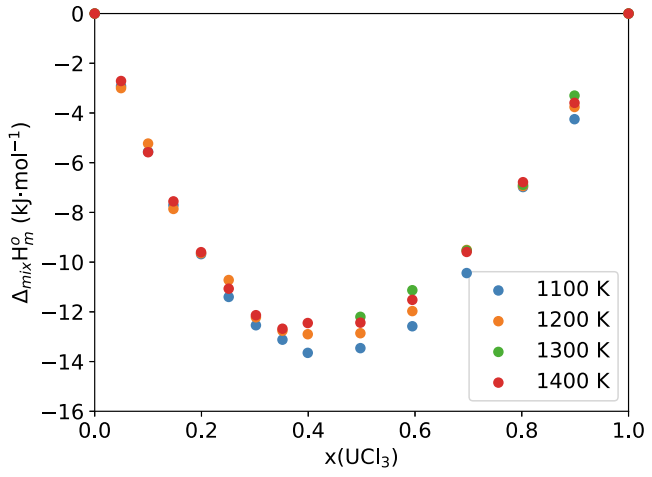

Fig. C.1. The mixing enthalpy of NaCl-UCl_3 as function of UCl_3 molar fraction at T = 1100, 1200, 1300 and 1400 K.

Appendix C. Mixing enthalpy

C.1

Appendix D. Supplementary material

Supplementary data associated with this article can be found, in the online version, at https://doi.org/10.1016/j.molliq.2021.117470.

References

[1] An Introduction to the Moltex Energy Technology Portfolio, Moltex Energy Ltd, Technical report, 2018.
[2] Advanced Reactors Information System (ARIS), Advances in Small Modular Reactor Technology Developments, IAEA, Technical report, 2018.
[3] A.T. Cisneros, K. Czerwinski, B.S. El-dasher, W.M. Kerlin, K. Kramer, J.F. Latkowski, R.C. Petroski, and J.C. Walter et al., Molten nuclear fuel salts and related systems and methods. June 30 (2016). US Patent App. 14/981,512.
[4] O. Beneš, R.J.M. Konings, Molten Salt Reactor Fuel and Coolant, in: Comprehensive Nuclear Materials, second ed., vol. 5, Elsevier, 2020.
[5] B. Li, S. Dai, D.E. Jiang, J. Mol. Liq. 299 (2020) 112184.
[6] A.A. Baty. Molecular dynamics simulation of the transport properties of molten transuranic chloride salts. Master's thesis, Texas A&M University, 2013.
[7] F.G. Edwards, J.E. Enderby, R.A. Howe, D.I. Page, J. Phys. C Solid State 8 (21) (1975) 3483.
[8] Y. Okamoto, P. Madden, K. Minato, J. Nucl. Mater. 344 (09) (2005) 109–114.
[9] H. Lukas, S.G. Fries, B. Sundman, Computational thermodynamics: the Calphad method, Cambridge University Press, 2007.
[10] H. Yin, J. Lin, B. Hu, W. Liu, X. Guo, Q. Liu, Z. Tang, Calphad 70 (2020) 101783.
[11] O. Beneš, R.J.M. Konings, J. Nucl. Mater. 375 (2) (2008) 202–208.
[12] A.L. Smith, E. Capelli, R.J.M. Konings, A.E. Gheribi, J. Mol. Liq. 299 (11) (2019) 112165.
[13] J.A. Ocadiz-Flores, A.E. Gheribi, J. Vlieland, K. Dardenne, J. Rothe, R.J.M. Konings, A.L. Smith, J. Mol. Liq. 331 (2020) 115820.
[14] C. Kraus. Phase Diagram of Some Complex Salts of Uranium with Halides of the Alkali and Alkaline Earth Metals, Office of Scientific and Technical Information, Technical report, 1943.
[15] E.S. Sooby, A.T. Nelson, J.T. White, P.M. McIntyre, J. Nucl. Mater. 466 (2015) 280–285.
[16] H. Matsuura, R. Takagi, L. Rycerz, M. Gaune-Escard, J. Nucl. Sci. Technol. 39 (2002) 632–634.
[17] V.N. Desyatnik, S.F. Katyshev, S.P. Raspopin, Y.F. Chervinskii, Sov. Atom Energy 39 (1) (1975) 649–651.
[18] F. Hutchinson, A.J. Rowley, M.K. Walters, M. Wilson, P.A. Madden, J.C. Wasse, P. S. Salmon, J. Chem. Phys. 111 (5) (1999) 2028–2037.
[19] W.J. Glover, P.A. Madden, J. Chem. Phys. 121 (15) (2004) 7293–7303.
[20] M. Salanne, C. Simon, P. Turq, P.A. Madden, J. Phys. Chem. B 112 (4) (2008) 1177–1183.
[21] C.W. Bale, E. Bélisle, P. Chartrand, S.A. Decterov, G. Eriksson, A.E. Gheribi, K. Hack, I.-H. Jung, Y.-B. Kang, J. Melançon, A.D. Pelton, S. Petersen, C. Robelin, J. Sangster, P. Spencer, M-A. Van Ende, Calphad 54 (2016) 35–53.
[22] V.P. Glushko, L.V. Gurvich, I.V. Weitz, V.A. Medvedev, G.A. Hachkuruzov, V.S. Jungmann, G.A. Bergman, V.F. Baibuz, V.S. Iorish, Nauka Publishing House, 1978.
[23] E. Capelli, R.J.M. Konings, Halides of the Actinides and Fission Products Relevant for Molten Salt Reactors, in: Comprehensive Nuclear Materials, second ed., vol. 7, Elsevier, 2020.
[24] B.C. Pyashyenko, Metallurgiya 10 (11) (1935) 85.
[25] W. Plato, Z. Phys. Chem. Leipzig 55 (1906) 721.
[26] I.G. Murgulescu, C. Telea, Rev. Roum. Chim. 22 (1977) 683.
[27] R. Dawson, E.B. Brackett, T.E. Brackett, J. Phys. Chem. 67 (1963) 1669.
[28] M.W. Chase Jr. J. Phys. Chem. Ref. Data, Monograph, NIST-JANAF thermochemical tables 9, 1998.
[29] A.D. Pelton, P. Chartrand, G. Eriksson, Metall. Mater. Trans. A 32 (6) (2001) 1409–1416.
[30] L.C. Dewan, C. Simon, P.A. Madden, L.W. Hobbs, M. Salanne, J. Nucl. Mater. 434 (1) (2013) 322–327.
[31] J. Wang, J. Wu, G. Lu, J. Yu, J. Mol. Liq. 238 (2017) 236–247.
[32] E.R. van Artsdalen, I.S. Yaffe, J. Phys. Chem. 59 (2) (1955) 118–127.
[33] M.B.J.W. Schreuder, J.A. Ocadiz-Flores, A.E. Gheribi, O. Beneš, J.-C. Griveau, E. Colineau, R.J.M. Konings, A.L. Smith, J. Phys. Chem. B 125 (2021) 8558–8571.